

Modulation transfer function and detective quantum efficiency of electron bombarded charge coupled device detector for low energy electrons

Miroslav Horáček^{a)}

Institute of Scientific Instruments, Academy of Sciences of the Czech Republic, Královopolská 147, CZ-61264 Brno, Czech Republic

(Received 22 December 2004; accepted 14 July 2005; published online 23 August 2005)

The use of a thinned back-side illuminated charge coupled device chip as two-dimensional sensor working in direct electron bombarded mode at optimum energy of the incident signal electrons is demonstrated and the measurements of the modulation transfer function (MTF) and detective quantum efficiency (DQE) are described. The MTF was measured for energy of electrons 4 keV using an edge projection method and a stripe projection method. The decrease of the MTF for a maximum spatial frequency of 20.8 cycles/mm, corresponding to the pixel size $24 \times 24 \mu\text{m}$, is $0.75 \approx -2.5$ dB, and it is approximately the same for both horizontal and vertical directions. DQE was measured using an empty image and the mixing factor method. Empty images were acquired for energies of electrons from 2 to 5 keV and for various doses, ranging from nearly dark image to a nearly saturated one. DQE increases with increasing energy of bombarded electrons and reaches 0.92 for electron energy of 5 keV. For this energy the detector will be used for the angle- and energy-selective detection of signal electrons in the scanning low energy electron microscope.

© 2005 American Institute of Physics. [DOI: 10.1063/1.2018587]

I. INTRODUCTION

The angular distribution of signal electrons, generated by the bombardment of crystalline surfaces or atomic steps or thin surface layers on bulk samples by the focused very low energy primary electron beam is inhomogeneous, exhibiting maxima and minima. The mechanisms responsible for angular distribution of signal electron beam are wave-optical phenomena, which can provide diffraction contrast, geometric phase contrast, and quantum size contrast.¹ These contrast mechanisms are well known and utilized in a non-scanning variant of the very-low energy electron microscopy (LEEM) if we use primary electrons of a wavelength comparable with the distance of atoms in the sample, i.e., very low energy electrons in the range of 10^0 – 10^1 eV. The first achievement of the diffraction contrast in a scanning electron microscope (SEM) with slow electrons was reported several years ago,² but with the yttrium–aluminum–garnet (YAG) crystal scintillator integrating an all dark-field signal around the optical axis and hence not acquiring the angular distribution of the backscattered electrons forming the diffraction contrast. Similarly, the image contrast in a SEM at low energies on differently doped areas in semiconductors exhibits angular distributions strongly different between the *p*- and *n*-type areas, which influences the contrast we are able to observe.³ The signal electrons escaping from the specimen under different angles can be processed by suitable electron optics to create the diffraction pattern on a multichannel planar detector. By repeating this within the scanned area in the SEM, the diffraction patterns can be recorded for every point of the

surface of the bulk sample studied. The image contrast of the surface is then obtained by processing the collected data.

The very low energy SEM with two-dimensional (2D) acquisition detector will be capable of revealing the angular distribution of emitted electrons and bringing a method of detection of signal electrons.

II. ACQUISITION OF ANGULAR DISTRIBUTION

The configuration of the scanning low energy electron microscope (SLEEM), which makes the angle-selective detection of signal electrons possible, has been described elsewhere.^{4,5} The signal electrons in SLEEM arrive at the detector with energy up to 5 keV. In order to acquire the angular distribution of signal electrons, we need a true 2D area detector. The image sensor based on a charge coupled device (CCD) chip is a standard solution for 2D acquisition. The sensor must fulfil main requirements such as the speed of the sensor, brightness resolution, dynamic range, and resistance to radiation damage. We have measured that the thinned back side directly electron bombarded CCD (EBCCD) chip has suitable parameters.⁴

For the detector speed, the key parameter of the EBCCD is the electron-bombarded semiconductor (EBS) gain G (a number of signal electrons in the potential well generated by one incident electron), which is related to the incident particle energy E . The dependence of gain on the energy is nonlinear for low energy below 10 keV. An electron with 4 keV energy generates about 300 electron–hole pairs (for 5 keV it is about 560); this value is connected with the material of a chip, so it is approximately the same for all silicon thinned back-side bombarded CCD. For the quality of image, the key parameters are dynamic range (saturation signal over spurious signals) and brightness resolution (the number of

^{a)}Electronic mail: mih@isibmo.cz

the gray levels resolvable in the image). The number of gray levels is equal to number of the incident electrons impinging on one pixel which generates N_c signal electrons in total in the potential well belonging to the pixel, where N_c is the well capacity of the CCD. Thus, the brightness resolution B is limited by the well capacity and CCD gain G , and it is given as $B=N_c/G$. For the usual well capacity of the CCD on the order of 10^5 and the gain on the order of 10^2 , the brightness resolution will be of $10^3 \approx 60$ dB. To achieve this brightness resolution, every potential well must be bombarded by $n = 1000$ electrons during integration time. Having the chip with 80×80 pixels with the illuminated central circular part containing 3490 pixels, we need the signal beam current $I_b = n \cdot e / T_{\text{int}} = 1000 \cdot 1.6 \times 10^{-19} \cdot 3490 / 5 \cdot 10^{-3} \approx 100$ pA to acquire one homogeneous angular distribution in integration time $T_{\text{int}} = 5$ ms. For the SEM image of 350×350 pixels we get ~ 10 min for the acquisition of the patterns from all points. The total time of 10 min is a maximum reasonable time from the point of view of operating efficiency and long term stability of the microscope. In the case of inhomogeneous angular distribution or diffraction patterns only some pixels of the pattern will be saturated. Therefore, the simple case of uniform distribution examined above is the worst case from the point of view of the total time and signal current.

Let us compare the gain of the thinned back-side EB-CCD and the gain of a CCD camera equipped with P20 or YAG for conversion of electrons and fiber optics as reducer to the CCD. This system was designed for transmission electron microscopes (TEMs), so only gain for high energy of 100 keV was presented, 780 with YAG and 142 with P20.⁶ We can estimate the gain 39, respectively, 7 for 5 keV. Another system with YAG and light optics has gain 3 for 5 keV.⁷ The integration time of such systems would be unusably long for the energy of signal electrons in SLEEM of 5 keV or less. On the contrary, the EBCCD in imaging tubes uses high gain of about 4000 at an operational voltage of 15 keV to make single electron detection possible.⁸ The brightness resolution of such a system is limited.

Cameras used in TEM do not use a CCD chip in a direct detection mode because exposure to fast electrons tends to degrade or destroy the CCD. On the contrary, in a SEM at 5 kV the risk of destroying the chip is negligible. Electrons below 5 keV do not degrade the CCD chip if we bombard the back side of the chip. This is why thinned back-side bombarded CCD sensors can be used in image intensifiers operating at 6 keV for more than 250 h.⁹ EBCCD operating at the voltage of 15 keV was successfully used in an image intensifier tube but without reporting the lifetime.⁸

Additional important characteristics of the image sensor are the modulation transfer function (MTF) and the detective quantum efficiency (DQE). Direct bombardment of a CCD chip, without any conversion elements like a YAG scintillator, and transfer elements like fiber optics, optical lenses, etc., should provide a better MTF of the detector. The DQE of the back-side illuminated EBCCD is expected to be comparable with systems using conversion elements. At the same time the integration time of the CCD can be below 10 ms. MTF and DQE were presented for slow-scan CCD cameras

for transmission electron microscopy where the signal electrons are converted into photons using scintillator or phosphor and CCD detects photons.^{6,10-12} The MTF of image intensifiers with electron bombarded CCD chips were measured only in an assembled image tube including a photocathode.⁹

Because we use the area array image sensor in a directly electron-bombarded mode, we have measured MTF and DQE of a direct electron bombarded CCD chip for an electron beam in the range up to 5 keV. Beside the speed of the sensor, a brightness resolution, and a dynamic range, the MTF and DQE are important parameters to decide if the thinned back-side directly electron bombarded CCD is a suitable detector for SLEEM.

III. MTF AND DQE OF ELECTRON-BOMBARDED CCD DETECTOR

The modulation transfer function is the key parameter to judge the ability of the image sensor to detect sharp transitions in luminance and periodically repeated transitions in luminance in the plane of the sensor. The modulation transfer function gives a relation of the peak output voltage of the sensor for stripe illumination to the output signal for homogeneous illumination, and it is defined by

$$\text{MTF} = \frac{U_{\text{pp}}(f_s)}{U_h}, \quad (1)$$

where $U_{\text{pp}}(f_s)$ is the peak-to-peak image signal under stripe illumination with the spatial frequency f_s and U_h is the image signal under homogeneous illumination. In electron microscopy, three methods for measuring the MTF are known: the edge method, the holographic method, and the stochastic method.¹³ The edge method calculates the MTF by the Fourier transform of the line-spread function (LSF) obtained from the edge-spread function (ESF) as¹⁰

$$\text{MTF} = F(\text{LSF}) = F(\text{ESF}'). \quad (2)$$

The detective quantum efficiency describes the ability of the sensor to transfer input image information into the output electrical signal from the point of view of added noise. The DQE is defined as

$$\text{DQE} = \frac{\left(\frac{S}{N}\right)_{\text{out}}^2}{\left(\frac{S}{N}\right)_{\text{in}}^2}, \quad (3)$$

where $(S/N)_{\text{out}}$ is the output signal-to-noise ratio and $(S/N)_{\text{in}}$ is the input signal-to-noise ratio. $(S/N)_{\text{out}}$ can be calculated from the image acquired by the sensor, while $(S/N)_{\text{in}}$ can be determined upon assumption that electrons in an electron beam obey the Poisson statistics. $(S/N)_{\text{in}}$ is therefore given as $N^{1/2}$, where N is the average number of incident electrons per pixel of the sensor. However, the direct calculation of the input signal-to-noise ratio from the electron beam statistics provides too high values of DQE. This is because we neglected the channel mixing (crosstalk) among neighboring pixels. If we neglect the channel mixing, we underestimate the input signal-to-noise ratio or overestimate the output

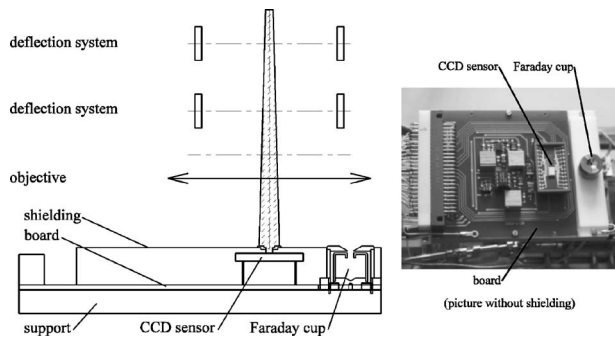


FIG. 1. Experimental setup. Final part of the optical system of SEM and sensor on specimen stage.

signal-to-noise ratio. The $(S/N)_{in}$ with channel mixing is given by¹¹

$$(S/N)_{in} = \sqrt{m \cdot N}, \quad (4)$$

where m is a mixing factor defined as

$$m = 1 / \sum_j f_{ij}^2, \quad (5)$$

where f_{ij} are mixing coefficients. A set of mixing coefficients $\{f_{ij}\}$ consist of j coefficients (one for every pixel), representing a fraction of electrons accumulated in the j th potential well, but generated by an electron impinging on the i th pixel; obviously it holds $\sum_j f_{ij} = 1$. The set of mixing coefficients is related to the point-spread function (PSF), which can be experimentally evaluated from direct measurement of the line spread function of the sensor. The relation between the line spread function and the point spread function is defined as

$$L_\mu = \sum_\nu P_{\mu\nu}, \quad (6)$$

where L_μ is LSF of line μ and $P_{\mu\nu}$ are PSFs of pixels along line μ .

IV. EXPERIMENTS AND RESULTS

All measurements presented here have been taken with a prototype of the position-sensitive directly bombarded detector of electrons.⁴ The detector is based on the back illuminated high performance CCD sensor CCD39-02 made by Marconi (80×80 pixels $\sim 1920 \mu\text{m}$ by $1920 \mu\text{m}$) working in the directly electron-bombardment mode. The measurements with the chip bombarded by electron beam were performed in a low energy SEM with a Schottky cathode, designed at the Institute of Scientific Instruments (accelerating voltage 0–5 keV, clean vacuum of 10^{-5} Pa in the chamber, PC-controlled optical system and specimen stage). The specimen chamber is large enough to accommodate the CCD sensor, amplifier, and Faraday cup of a picoammeter on the x - y translation stage inside the chamber, and it is equipped with two sufficiently large multipin feedthroughs to connect the sensor with the electronics. The main electronics is situated outside the vacuum. The schematic arrangement of the experimental configuration and a photograph of the board are presented in Fig. 1. The image area of the sensor was positioned directly under the primary electron beam. The electron beam was defocused by switching off the objective lens,

in order to create a homogeneous electron illumination on the image area of the sensor. The storage area of the sensor and on-chip amplifier were protected against electrons by a Cu shielding having a round hole only above the image area of the sensor.

Every measurement followed the next procedure: we moved the Faraday cup with a hole of 1.6 mm diameter under the electron beam and measured the beam current I_b . Next, we moved the shielded CCD sensor with a hole of the same diameter under the electron beam and measured the detected output signal U_{out} as a function of the integration time T_{int} for every pixel of image matrix, i.e., we acquired one image or set of images.

A. MTF measurement using edge projection method

In order to generate a sharp transition in luminance on the sensor we modulated the source of luminance (electron beam in our case) by an edge. The edge was created by one side of a slot (oval hole 2×1 mm). The slot was stuck on a Cu holder with the central hole of 1.6 mm in diameter. The holder with the slot was mechanically inserted into the shielding and the slot was situated approximately 1 mm above the sensor surface. The energy of the impinging electrons was set on $E=4$ keV, for which the EBS gain of the CCD sensor is ~ 300 . This is close to the optimum working value for the EBCCD detector, so we measured the MTF under the conditions planned to be used in practice.⁴ The sensor was bombarded with electron beam of ~ 5 nA/cm². Two measurements were made, namely with the edge of the slot oriented perpendicular and parallel to the serial register of the CCD, in order to measure the horizontal and vertical MTF, respectively. The edge spread function is obtained as a line scan in the image of the edge projection on the sensor. Then we used the standard procedure to calculate the MTF [Eq. (2)]: edge spread function \Rightarrow derivative \Rightarrow line spread function \Rightarrow Fourier transform \Rightarrow MTF. The calculation was made by MATLAB.

To acquire the best edge spread function, the edge of the slot must be positioned exactly above the boundary between two lines (for the vertical MTF measurement) or columns (for the horizontal MTF measurement) of pixels. To adjust this setting, we would have to move the slot independently against the CCD sensor. However, because the slot was fixed with the shielding and the shielding with the printed circuit board of the sensor, we could not move the slot and sensor against each other in the microscope chamber during the measurement. So we moved the edge of the electron beam by fine tilting ($\pm 1^\circ$) the whole configuration situated on the specimen stage (see Fig. 1). Several sets of images of the slot (every set measured for integration times T_{int} from a nearly dark image to a saturated image) was measured for several tilts in both the perpendicular and parallel orientation of the slot. The two best half-line scans (one horizontal and one vertical) were used for the MTF's computation. The images of the slot with marked half lines, used for the MTF computation, are shown in Fig. 2. The vertical MTF is presented in Fig. 7 (line) and the horizontal MTF is approximately the same.

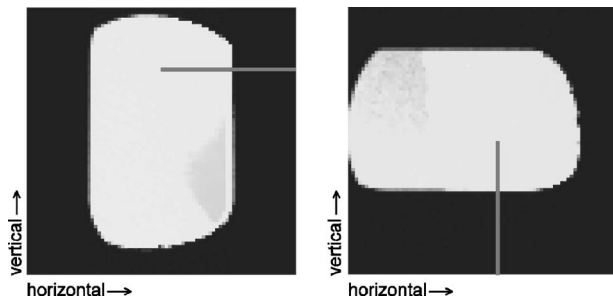


FIG. 2. e -beam images of slots with marked half lines, used for the MTF computation: $E=4$ keV, $T_{\text{int}}=6$ ms, $I_b=100$ pA.

The decrease in the MTF for maximum spatial frequency 20.8 cycles/mm, which corresponds to a pixel size of $24 \times 24 \mu\text{m}$, is $\text{MTF}(20.8)=0.75 \approx -2.5$ dB and it does not differ between horizontal and vertical directions. Therefore, the decrease in the dynamic range of sharp transitions in the electron beam image is within standard limits of $0.71 \approx -3$ dB. The reason for this very good result is the fact that there are no other optical components in the detection channel, like scintillator, fiber optics, glue etc., which could degrade the MTF of the CCD.

B. MTF measurement using stripe projection method

In order to verify the results obtained by the edge projection method, we projected onto the sensor a pattern made of stripes; in practice we modulated the electron beam by rectangular meshes of various dimensions. This method follows directly from the definition of the MTF [Eq. (1)]. We projected the mesh only on one half of the image area of the sensor and simultaneously a nonmodulated electron beam image on the second half of the image area. A round mesh was cut in halves and one of them was stuck to the Cu holder. In this way we eliminate the fluctuations in the electron beam current density and obtain both quantities in Eq. (1) under the same illumination conditions.

In order to fulfill the strict conditions governing measurement of the modulation transfer function with the stripe projection method, we have to use stripe patterns of spatial frequencies exactly corresponding to the pixel size $24 \mu\text{m}$ of the sensor. The maximum spatial frequency is $1/(2 \times 24 \cdot 10^{-3})=20.8$ cycles/mm. Because our sensor has 80×80 pixels, the minimum useable spatial frequency is 0.52, corresponding to one illuminated stripe 40 pixels wide and one dark (shielded) stripe of the same width. The stripe distributions must be projected onto the sensor in such a way that their edges are positioned exactly above the boundaries between two lines (for the vertical MTF measurement) or a column (for the horizontal MTF measurement) of pixels. This condition must be fulfilled especially for measurements at high spatial frequencies. Because we use this method only for verification of the results of the edge method, we incorporated a simplified solution. We used three rectangular meshes with different dimensions: (1) period $125 \mu\text{m}$, hole $90 \mu\text{m}$; (2) period $85 \mu\text{m}$, hole $50 \mu\text{m}$; and (3) period $65 \mu\text{m}$, hole $40 \mu\text{m}$. We calculated the spatial frequency from the mesh period and neglected the difference between period and hole dimensions.

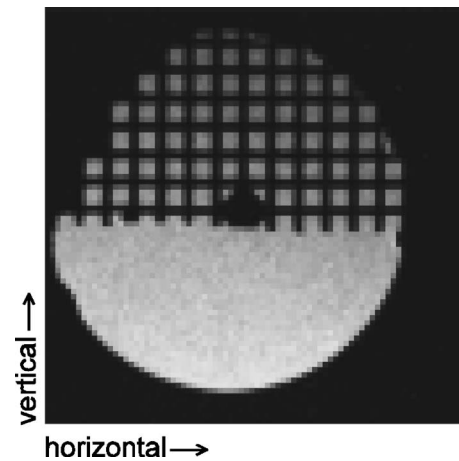


FIG. 3. e -beam image of mesh, used for the MTF computation: $E=4$ keV, $T_{\text{int}}=8$ ms, $I_b=60$ pA.

An example of the e -beam image of the halved mesh in Fig. 3 corresponds to $f_s=8.0$ cycles/mm, and its vertical line scan in Fig. 4 is used to obtain $U_{\text{pp}}(f_s)$ and U_h for the calculation of the vertical MTF. Vertical line scans for the other two meshes are shown in Fig. 5 ($f_s=11.8$ cycles/mm) and Fig. 6 ($f_s=15.4$ cycles/mm). The values of $U_{\text{pp}}(f_s)$ for the calculation of the horizontal MTF can be obtained from horizontal line scans across the same meshes, with corresponding values of U_h taken from Figs. 4–6. Values for the horizontal MTF can also be acquired from single line scans when rotating the meshes by 90° . The measured values of MTF are presented in Fig. 7 (stars).

Because we project squares instead of stripes on the sensor, the image is smeared in both directions, i.e., the horizontal and vertical ones. This effect must be taken into account when comparing the results from the edge and stripe methods. To estimate the value of the MTF measured using the stripe projection method from data acquired by the edge method, we simply multiply the horizontal MTF by the vertical MTF (obtained from the line in Fig. 7) for three spatial frequencies used (8.0, 11.8, and 15.4 cycles/mm). In this way we get (0.92, 0.83, and 0.72) while from Figs. 4–6 we

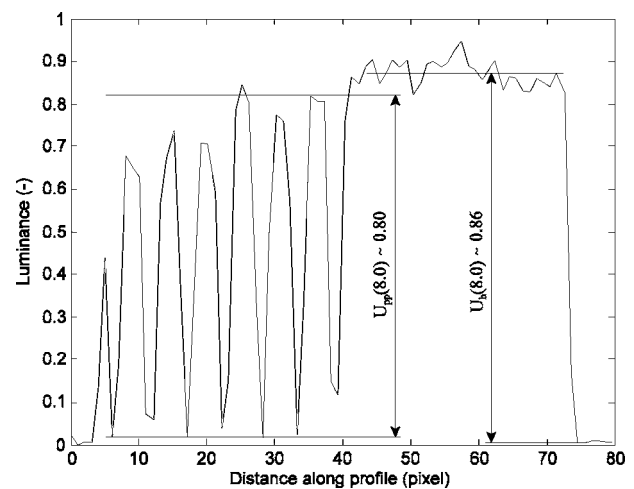


FIG. 4. Vertical line scan of image of mesh (step $125 \mu\text{m}$, hole $90 \mu\text{m}$, $f_s=8.0$ cycles/mm).

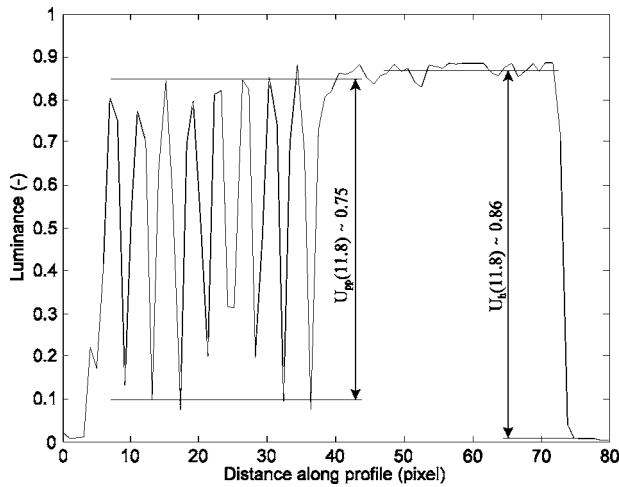


FIG. 5. Vertical line scan of image of mesh (step $85 \mu\text{m}$, hole $50 \mu\text{m}$, $f_s = 11.8$ cycles/mm).

calculated (0.93, 0.87, and 0.64). The values are approximately the same for both directions. The main reason is the square shape of the pixels. The values measured using the stripe method are lower than those produced by the edge method because in fact we used a square so the charge generated in the potential well is smeared in both directions. As a result, the amplitudes of the line scans in Figs. 4–6 are lower.

The reasons for the difference between the measured and estimated data include: (1) mesh edges are not positioned exactly above the boundaries between pixels—this reduced the measured value especially for the finest mesh and (2) inhomogeneous current density in the beam—this makes the signal amplitude fluctuate along the line.

C. DQE measurement using empty image and mixing factor method

In this series of measurements, we projected onto the sensor an empty, i.e., nonmodulated, image. The defocused electron beam was only trimmed to the diameter of 1.6 mm by the Cu holder inserted into the shielding. Seven sets of

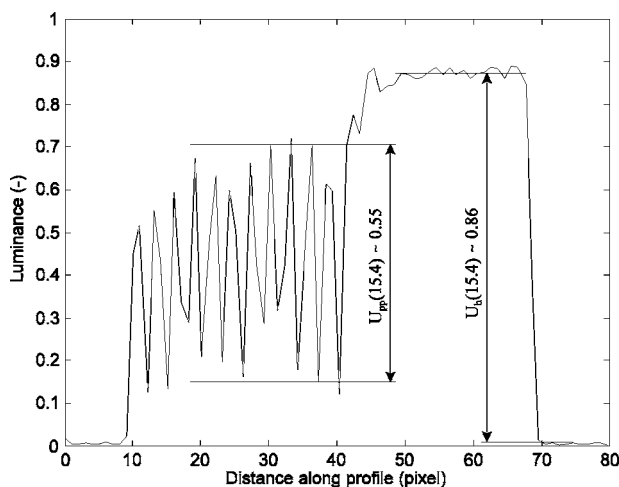


FIG. 6. Vertical line scan of image of mesh (step $65 \mu\text{m}$, hole $40 \mu\text{m}$, $f_s = 15.4$ cycles/mm).

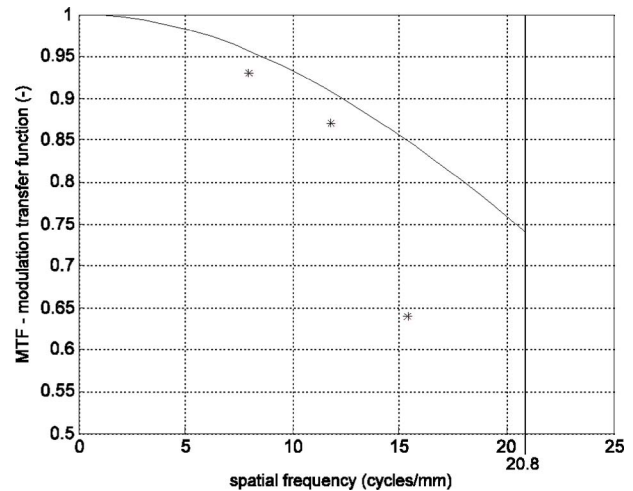


FIG. 7. MTF of the electron bombarded CCD for energy of electrons 4 keV (line—edge method; stars—stripe method).

images for electron energy between 2 and 5 keV were acquired. For every measurement the beam current, measured by the Faraday cup, was set to approximately the same level. Each set contains several images with different doses ranging from a nearly dark image to a nearly saturated image. The dose was controlled by the integration time.

The output signal-to-noise ratio $(S/N)_{\text{out}}$ was calculated from a ratio of the average image signal within a matrix of 10×10 pixels in the chip center and the standard deviation over the same matrix of pixels. The central part of the image area was chosen in order to avoid effects of inhomogeneous current density. The dark current was subtracted from mean values of the images. $(S/N)_{\text{in}}$ was calculated from Eq. (4). The average number of incident electrons per pixel was calculated as $N = (I_b \cdot T_{\text{int}}) / (e \times 3490)$, where I_b is the current measured by the Faraday cup, T_{int} is the integration time, e is the electron charge, and 3490 is the number of pixels within the diameter of 1.6 mm. Mixing coefficients were calculated by fitting the estimated discrete PSF to the line-spread function of the sensor, as measured above for the MTF calculation. Next we normalized the discrete values of PSF and calculated the mixing factor from Eq. (5). The resulting value of the mixing factor, $m = 1.15$, is very low. This factor is related to the ability of a the CCD chip to detect sharp transitions in luminance. The final DQE was then obtained from Eq. (3). All calculations were made by MATLAB.

The values of DQE for different electron energies are plotted in Fig. 8 with respect to the number of incident electrons per pixel. Because for every measurement the beam current was set to the same level of 100 pA, we can compare in single graph the DQEs for different energies. The horizontal axis can be simply recalculated into the integration time, for example $N = 10^3 \sim T_{\text{int}} = 5.6$ ms. DQE obviously increases with the increasing energy of electrons. The denominator of Eq. (3), i.e., $(S/N)_{\text{in}}$, is constant for the fixed number of incident electrons, but the numerator increases with increasing energy. This is why the multiplication process of creation of electron-hole pairs in the Si chip during the electron bombardment exhibits fluctuations with a standard deviation of $\sigma = (F \cdot G)^{1/2}$, where F , the Fano factor, is 0.12 in silicon and

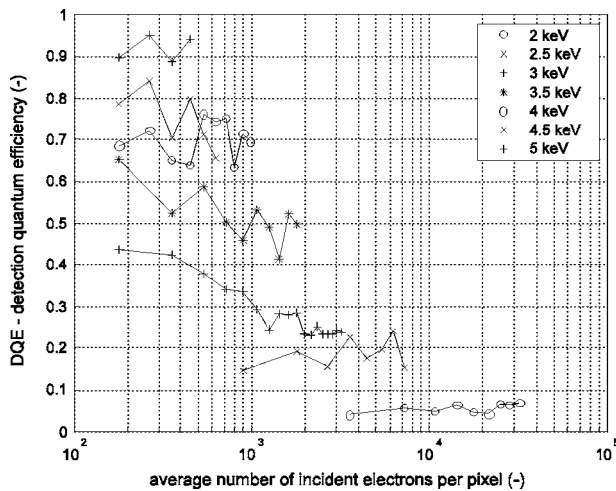


FIG. 8. DQE of the electron bombarded CCD for energies of electrons 2–5 keV.

G is an electron bombarded semiconductor gain of the CCD chip.¹⁴ The gain grows with the increasing energy of electrons, but the increase in the standard deviation is much slower, so $(S/N)_{\text{out}} \sim G/\sigma$ increases.

Taking into account the spurious signals of the chip as the dark signal, dark signal nonuniformity, and readout noise, we measured the dynamic range of the sensor equal to 890 \approx 59 dB at room temperature for integration time below 10 ms. The dynamic range is practically constant for these T_{int} . This is because the dynamic range for low integration time is limited mainly by the readout noise of the CCD. Should this dynamic range be fully utilized, we must work with a brightness resolution on the same level 890. To achieve this brightness resolution, the CCD sensor CCD39-02 with well capacity of the chip 300×10^3 electrons must work with gain $G = N_c/B = 300 \times 10^3/890 \approx 340$. Such gain is achieved at incident particle energy $E \approx 4.2$ keV.⁴ The energy of the incident signal electrons in the EBCCD detector plane can be independently adjusted in SLEEM to set an optimum gain. We can see from Fig. 8 that DQE ≈ 0.7 for 4.2 keV. Thus 0.7 is the maximum value of detective quantum efficiency useable for the EBCCD detector. It makes no sense to increase the DQE by bombardment of the chip by higher energy electrons, because we would reduce

the brightness resolution. Let us remember that no cooling of the chip was used during measurements. Using the Peltier cooler we can further reduce the spurious signals and consequently increase the dynamic range and DQE at the same incident particle energy. In order to utilize the higher dynamic range we can decrease the gain to utilize a higher brightness resolution. But the integration time will be longer. We can see that all parameters are interconnected and must be tailored to a specific application.

The CCD chip can work successfully as an image sensor in direct electron bombarded mode if we use a thinned back-side illuminated version of the CCD and if we adjust optimum energy of the incident signal electrons. EBCCD is the solution for fast application of the area detector in low energy electron optical devices. We optimized our detector for acquisition of 2D angular distribution of signal electrons in a scanning low energy electron microscope. The utilization of this detector will provide new image contrast information and it can introduce new methods for examination of clean surfaces.

ACKNOWLEDGMENTS

The work was supported by the Grant Agency of the Czech Republic under Grant No. 202/03/1575. The contributions of Professor B. Lencová and Dr. I. Müllerová to the manuscript are gratefully acknowledged.

¹E. Bauer, Rep. Prog. Phys. **57**, 895 (1994).

²L. Frank, I. Müllerová, K. Faulian, and E. Bauer, Scanning **21**, 1 (1999).

³I. Müllerová, M. M. El-Gomati, and L. Frank, Ultramicroscopy **93**, 223 (2002).

⁴M. Horáček, Rev. Sci. Instrum. **74**, 3379 (2003).

⁵M. Horáček, J. Comput-Assist. Microsc. **10**, 23 (1998).

⁶S. Kujawa and D. Krahl, Ultramicroscopy **46**, 395 (1992).

⁷R. Sikeler and K. H. Herrmann, Proceedings 13th ICEM, Paris, 1994, p. 217.

⁸S. Buontempo *et al.*, Nucl. Instrum. Methods Phys. Res. A **413**, 255 (1998).

⁹W. Enloe, R. Sheldon, L. Reed, and A. Amith, Proc. SPIE **1655**, 41 (1992).

¹⁰A. L. Weickenmeier, W. Nüchter, and J. Mayer, Optik **99**, 147 (1995).

¹¹K. Ishizuka, Ultramicroscopy **52**, 7 (1993).

¹²O. L. Krivanek and P. E. Mooney, Ultramicroscopy **49**, 95 (1993).

¹³C. Hülk and I. Daberkow, Proceedings 14th ICEM, Cancun, 1998, Vol. I, p. 189.

¹⁴W. van Roosbroeck, Phys. Rev. **139**, A1702 (1965).